

Effect of Particle Size on the Oxidizability of Platinum Clusters

Ye Xu,[†] William A. Shelton,[†] and William F. Schneider^{*,‡}

Computer Science and Mathematics Division, Oak Ridge National Laboratory, Oak Ridge, Tennessee 37831, and Department of Chemical and Biomolecular Engineering, and Department of Chemistry and Biochemistry, University of Notre Dame, Notre Dame, Indiana 46556

Received: August 21, 2005; In Final Form: February 16, 2006

The catalytic properties of transition metal particles often depend crucially on their chemical environment, but so far, little is known about how the effects of the environment vary with particle size, especially for clusters consisting of only a few atoms. To gain insight into this topic, we have studied the oxygen affinity of free Pt_x clusters as a function of cluster size ($x = 1, 2, 3, 4, 5$, and 10) using density functional theory (DFT) calculations (GGA-PW91). DFT-based Nosé–Hoover molecular dynamics has been used to explore the configuration space of the Pt_xO_x and Pt_xO_{2x} clusters, leading to the discovery of several novel Pt–oxide structures. The formation of small Pt–oxide clusters by oxidizing the corresponding Pt_x clusters is found to be significantly more exothermic than the formation of bulk Pt–oxides from Pt metal. The exothermicity generally increases as cluster size decreases but exhibits strongly nonlinear dependence on the cluster size. The nanoclusters are also structurally distinct from the bulk oxides and prefer one- and two-dimensional chain and ringlike shapes. These findings help elucidate the oxidation behavior of Pt nanoclusters and lay the foundation for understanding the reactivity of Pt nanoclusters in oxidizing chemical environments.

Introduction

Heterogeneous catalysis by oxide-supported transition metals is crucial to the modern chemical and energy industries. The most versatile transition metal is arguably platinum (Pt), which catalyzes many oxidation, reduction, and reforming processes. For instance, Pt is currently the preferred anode (oxidation) and cathode (reduction) catalyst for low-temperature PEM fuel cells.¹ Pt also figures prominently in catalytic aftertreatment technologies that protect the environment, such as the automotive three-way catalytic converter, in which CO, NO_x, and unburned hydrocarbons are converted to the more benign CO₂, H₂O, and N₂ simultaneously, and the lean NO_x trap, in which Pt is used to catalyze oxidations under strongly oxidizing conditions.^{2,3}

In most of the catalytic applications of Pt, the metal is deployed as minute particles, a few nanometers in diameter, finely dispersed on a high surface-area supports.⁴ This is because Pt is expensive and because smaller Pt particles tend to be more catalytically active. The enhanced activity has generally been explained in terms of the increased surface areas of smaller particles and the structural sensitivity of some reactions. The striking ability of Au to catalyze a number of important reactions, including CO oxidation, partial oxidation of propylene, and hydrogenation of unsaturated hydrocarbons, only in highly dispersed forms⁵ highlights the importance of understanding the reactivity of small metal particles on the atomic level. With the help of theoretical methods such as density functional theory (DFT), the roles of under-coordinated sites,⁶ particle-support interface,⁷ altered oxidation state,⁸ and quantum size effects⁹ have been examined in Au catalysis. Notable progress has also

been made for several other catalytic systems,^{10,11} although detailed knowledge is still lacking for many.

Laboratory techniques are now available for synthesizing clusters consisting of a handful of atoms from evaporated metals¹² or organometallic precursors.^{13,14} This ability to control particle size has spurred new research efforts aimed at engineering size-specific reactivity, something especially relevant for Pt for the aforementioned reasons. Supported nanocluster catalysts of Re,¹⁵ Os,¹⁶ Rh,¹⁷ Ir,^{18,19} Pt,^{20–22} and Au^{23,24} have been reported in the literature. However, knowledge of how supported metal particles interact with the chemical environment, which includes variables such as temperature and pressure, gas-phase and surface species, and the nature of the support, remains scanty. One manifestation of the problem is the so-called “pressure gap”. With combined experimental and theoretical efforts, Scheffler and co-workers and King and co-workers have recently related the reactivity of Ru in CO oxidation catalyst^{25,26} and Ag in ethylene epoxidation to the formation of surface oxides under reaction conditions.^{27–29} Existing experimental evidence suggests that Pt is found predominantly in oxidized forms in an oxidizing environment.^{30–33} Recent high-pressure surface science experiments on ordered Pt surfaces provide convincing evidence that the presence of metastable surface oxides significantly enhance CO oxidation activity.^{34–37} Because Pt is commonly used as an oxidation catalyst, it is important to understand the structural, energetic, and catalytic properties of finite Pt nanoclusters under an oxidizing vs. a reducing environment. This knowledge may also benefit the study of sintering behavior of small Pt particles.³⁸

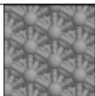
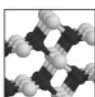
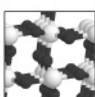
Metal clusters supported on metal oxides and exposed to gaseous environments comprise functionally rich but complex systems, the analysis and modeling of which require careful consideration. In this study, we take the first step by using DFT calculations to study a series of Pt_xO_x and Pt_xO_{2x} clusters ($x = 1, 2, 3, 4, 5$, and 10). We investigate the energetics of the

* To whom correspondence should be addressed. William F. Schneider, 182 Fitzpatrick Hall, University of Notre Dame, Notre Dame, IN 46556. E-mail: wschneider@nd.edu.

[†] Oak Ridge National Laboratory.

[‡] University of Notre Dame.

TABLE 1: Structural Parameters of Bulk Pt Metal, PtO, and β -PtO₂^a

Bulk	space group	calculated lattice constant(s) (Å)	exp. lattice constant(s) (Å)		
Pt	Fm3m	4.00	3.92	Ref. 50	
PtO	P4 ₁ /mmc	$a = 3.143$	$a = 3.08$	Ref. 30	
		$c = 5.443$	$c = 5.34$		
β -PtO ₂	Pnnm	$a = 4.62$	$a = 4.484$	Ref. 51	
(CaCl ₂ prototype)		$b = 4.58$	$b = 4.539$		
		$c = 3.19$	$c = 3.136$		
		$x = 0.26$	$x = 0.267$		
		$y = 0.36$	$y = 0.350$		

^a Experimental values are included for comparison; x and y refer to the fractional positions of the O atom.

oxidation of free Pt_{*x*} nanoclusters and the preferred structures and oxidation states of the resultant Pt–oxide nanoclusters. The results provide insights into how supported Pt nanoclusters can respond to an oxidizing environment and give guidance for future, more detailed investigations. In addition, the nanoclusters that we explore offer probable structural models of the active sites of extended Pt–oxide surfaces.³⁹

Methods

The periodic spin-polarized DFT calculations are performed using the Vienna Ab-initio Simulation Package (VASP)^{40–43} in the generalized gradient approximation (GGA). The exchange–correlation energy and potential are described by the PW91 functional.⁴⁴ The ionic cores are described by Vanderbilt’s ultrasoft pseudopotentials.⁴⁵ The Kohn–Sham valence states are expanded in a plane-wave basis up to a kinetic energy of 396 eV. To accelerate convergence, electronic states are smeared using a Gaussian scheme ($k_B T = 0.01$ eV). The final electronic states all have unit occupancies, as required for discrete molecular clusters. As the intent is to simulate isolated clusters, k space is sampled at the Γ point only. Clusters are calculated within a cubic $18 \times 18 \times 18 \text{ \AA}^3$ unit cell, which is sufficiently large so that the electrostatic interaction among periodic images does not affect the total energy of a system to more than a few meV. Reciprocal space integration is done on a $120 \times 120 \times 120$ FFT grid to avoid wrap-around error. The ground-state spin multiplicity of each cluster is verified. Structures are relaxed until the maximum force on any atom is less than 0.01 eV/\AA .

For reference we have calculated the bulk Pt metal and two bulk Pt–oxides, PtO and β -PtO₂ (the stable phase under elevated pressure). A $16 \times 16 \times 16$ Monkhorst-Pack k -point mesh is used for the bulk calculations. The occupancies of electronic states are determined using the tetrahedron method with Blöchl corrections.⁴⁶ The same kinetic energy cutoff of 396 eV is used as above. These parameters are sufficient for the total energy to converge to a few meV. The calculated structural parameters are shown in Table 1 (in the insets and hereafter, light and dark spheres represent Pt and O atoms, respectively). As can be seen, DFT tends to overpredict the lattice constants, which is a known deficiency of the GGA, but

the difference is generally less than 4% of the experimental values. For bulk Pt, the cohesive energy (with respect to a spherically symmetric free Pt atom, which is also used in calculating the atomization energies of the Pt_{*x*} clusters later) and bulk modulus are found to be 5.52 eV and 233 GPa, respectively. The corresponding experimental values are 5.85 eV⁴⁷ and 228 GPa.⁴⁸

The calculated heats of formation for bulk PtO and β -PtO₂ are -0.55 and -1.57 eV/Pt, respectively, with respect to bulk Pt metal and an O₂ molecule. Our values differ from the tabulated standard heats of formation of the two oxides (-0.74 and -1.39 eV/Pt,⁴⁹ respectively) by less than 0.2 eV. In analogy to the definition of the heat of formation for the bulk oxides, we define the formation energy (FE) of a Pt_{*x*}O_{*y*} cluster as:

$$\text{FE}_{\text{Pt}_x\text{O}_y} = (E_{\text{Pt}_x\text{O}_y} - E_{\text{Pt}_x} - \frac{1}{2}y \cdot E_{\text{O}_2})/x$$

Here, $E_{\text{Pt}_x\text{O}_y}$ is the total energy of a Pt_{*x*}O_{*y*} cluster, E_{Pt_x} is the total energy of the minimum-energy configuration for the Pt_{*x*} cluster, and E_{O_2} is the total energy of an O₂ molecule. As will be seen later, an absolute error of less than 0.2 eV is also found for the FE’s of the PtO and PtO₂ molecules, suggesting errors of similar magnitude in the calculated FEs of structures intermediate in size between molecular and bulk PtO and PtO₂.

To determine the lowest FE for each of the Pt_{*x*}O_{*x*} and Pt_{*x*}O_{*2x*} clusters is tantamount to finding the structure located at the global minimum on the potential energy surface (PES) of a cluster. To date, although a number of algorithms have been developed to address the challenge of locating the global minimum on a multidimensional surface (e.g., simulated annealing, basin hopping Monte Carlo, and genetic algorithms), none yet offers a guaranteed solution. Furthermore, no reliable empirical potentials for Pt and O in small Pt–oxide clusters are available, which substantially limits the ability of many of those algorithms to converge to low-energy structures automatically. For a small Pt–oxide cluster, the number of stable structures (local minima) is finite and can be exhaustively investigated by manually constructing a number of trial structures. However, as the cluster size increases, the number of local minima on the PES grows quickly, making a manual search untenable.

For a Pt–oxide cluster that contains more than 5–6 atoms, therefore, DFT-based Nosé–Hoover molecular dynamics (MD)⁵² is used to assist in the search for candidate structures for further optimization. The DFT parameters in the MD calculations are less stringent than those used in geometry optimization (kinetic energy cutoff of 150 eV and Gaussian smearing temperature of 0.1 eV). The MD parameters, including the Nosé–Hoover thermostat (0.1), initial temperature (500–750 K), and time step (0.5–1.0 fs), are all chosen to facilitate the rapid sampling of large portions of the configuration space of the cluster over several thousand time steps. The evolution of the total energy is monitored, and low-energy structures are further converged or used to guide the construction of new trial structures. In the end, the structure with the lowest energy is regarded as the most stable structure of the given composition Pt_{*x*}O_{*y*}. The consistent structural patterns and the clear trends in the calculated FE give us the confidence that the structures reported below either are the global minima for each composition or are energetically very close to them.

The vibrational frequencies of the clusters are calculated in the harmonic approximation for comparison with available experimental measurements and for calculating the zero-point energies (ZPE’s) of the clusters. The second derivatives of

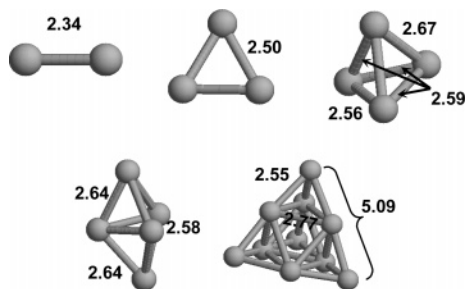


Figure 1. From left to right: the Pt₂, Pt₃, and Pt₄, (first row) Pt₅, and Pt₁₀ (second row) clusters. Lengths of selected bonds (in Å) are indicated.

energy are determined using central-differencing approximation (with a 0.01 Å displacement) and used to construct the mass-weighted Hessian matrix, which is then diagonalized to give the normal modes of a cluster, the eigenvalues associated with which are the vibrational frequencies of the cluster. For a linear cluster, there are $3n - 5$ normal modes, where $n = x + y$. For a nonlinear cluster, there are $3n - 6$ normal modes. If we define $\Theta_{vi} = \hbar\nu_i/k_B$ as the characteristic vibrational temperature of each normal mode i , then

$$\text{ZPE} = \frac{1}{2} \sum_i k_B \Theta_{vi}$$

Here k_B is the Boltzmann constant. The ZPE correction is less than 0.05 eV/O for all Pt–oxide clusters considered in this study. The calculated O–O stretching frequency is 1571 cm^{−1}, in very good agreement with the 1580 cm^{−1} listed by NIST.

Besides the energetic and structural properties, the oxidation states of the atoms in the Pt–oxide clusters are also of interest because the oxidation state is often a key factor in determining the chemical reactivity of metal oxides. Bader charge partition analysis⁵³ is done using the code developed by Henkelman et al.⁵⁴ to determine the number of electrons transferred to and from each atom in a cluster, which will be used as a proxy for oxidation state.

Results

Pt Clusters. Before investigating the Pt–oxide clusters, we first determine the properties of the pure Pt_x clusters, which will be used as reference states for calculating the FE of the Pt–oxide clusters. Our calculations are guided by the results of a number of previous theoretical studies.^{55–60}

The ground-state Pt dimer is a triplet with an atomization energy (AE) of 1.82 eV/Pt or 3.64 eV total. The calculated Pt–Pt bond length (see Figure 1) and vibrational frequency (220 cm^{−1}) agree closely with the experimentally measured values of 2.33 Å⁶¹ and 215 cm^{−1}.⁶² The calculated AE shows overbinding compared to the 3.14 eV measured by Tayler et al. using resonant two-photon ionization spectroscopy.⁶³ The Pt trimer prefers to form an equilateral triangle with D_{3h} symmetry.^{56,57} The ground state of this geometry is also a triplet with an AE of 2.43 eV/Pt. Previous theoretical studies indicate that the lowest energy structure of Pt₄ is a slightly distorted tetrahedron with D_{2d} symmetry.^{57,60,64} De Silva et al. report that the tetrahedron has Pt–Pt bonds of two different lengths, 2.56 and 2.67 Å, and that the ground state is a triplet.⁶⁴ Our calculations give essentially the same results. The AE of Pt₄ is 2.74 eV/Pt. For the minimum-energy structure of Pt₅, Majumdar et al. reported a distorted tetragonal pyramid, which is less than 0.1 eV more stable than a regular trigonal bipyramid, in a

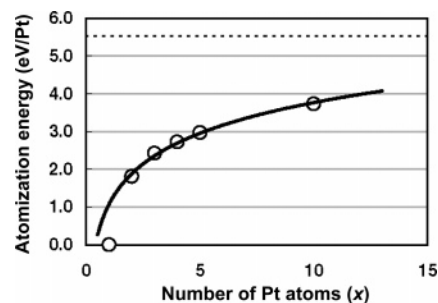


Figure 2. Calculated, ZPE-corrected atomization energy (AE) of the Pt_x clusters (O) and cohesive energy of bulk Pt (5.52 eV/Pt, dashed line).

CASMCSCF-MRSDCI study.⁵⁶ Within the accuracy of our calculations, we find that the trigonal bipyramid (D_{3h} symmetry) is 0.19 eV more stable than the tetragonal pyramid. The ground state of this bipyramid cluster is a quintet with an AE of 2.98 eV/Pt, which agree closely with the findings of Xiao et al.⁶⁰ The Pt₁₀ cluster prefers a regular tetrahedron geometry (T_d symmetry).^{57,60} Its ground state is a nonet and has an AE of 3.75 eV/Pt. Each face of the tetrahedron resembles a small patch of the extended Pt(111) surface. The ZPE reduces the AE by no more than 0.02 eV/Pt for all six clusters.

The calculated atomization energy increases monotonically with cluster size (see Figure 2). The fact that the Pt atoms are held together more strongly as the size of the cluster increases has been noted before.^{55,59,60} The same behavior has also been reported for Pb nanoparticles supported on MgO.³⁸ The atomization energy can be approximately fitted to the function $AE = 1.174 \cdot \ln(x) + 1.080$ ($r^2 = 0.99$) for the five calculated clusters (Pt_{2,3,4,5,10}), with a root-mean-square error of 0.21 eV. This log function is not asymptotically correct but is useful for estimating the AE of other small Pt_x clusters, which we take advantage of below. Incidentally, it has been pointed out that the AE's of the Pt nanoclusters are substantially higher than clusters of the other Group 10 metals (Ni and Pd) containing the same number of atoms.⁵⁵ This trend has been attributed to large relativistic effects in the Pt electronic structure that enhance d orbital contributions to Pt–Pt bonding.⁶¹

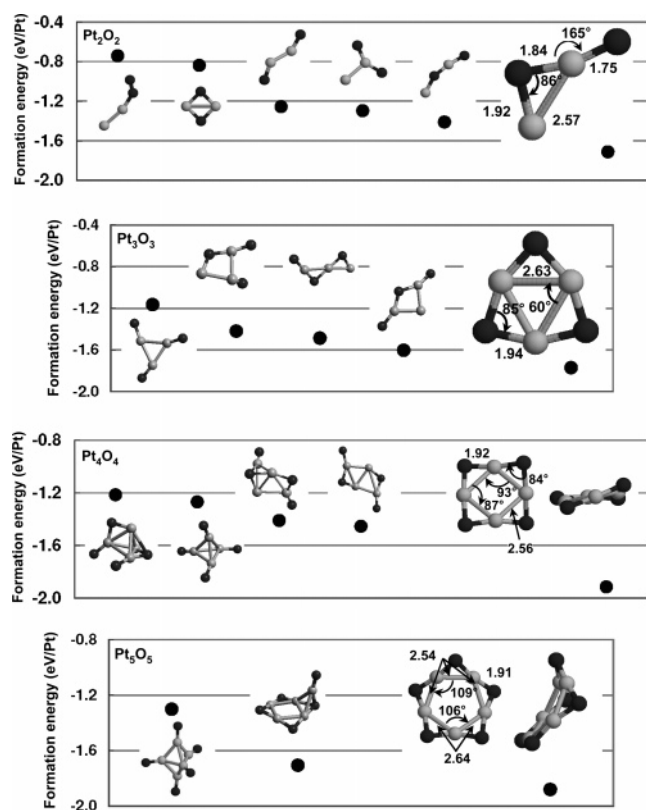
Pt–Oxide Clusters. The most common Pt oxidation states are 2+ and 4+, as reflected both in its coordination chemistry and principle bulk oxides. Here, we focus on these oxidation states and investigate Pt–oxide nanoclusters with Pt_xO_x and Pt_xO_{2x} stoichiometries ($x = 1, 2, 3, 4, 5$, and 10), including their electronic, structural, and energetic properties as a function of x . ZPE-corrected FE's of the clusters are included in curly brackets.

Pt_xO_x Clusters. The smallest Pt_xO_x cluster, the PtO molecule, is a triplet in the ground state (Table 2). It has a bond length of 1.76 Å and stretching frequency of 812 cm^{−1}, and its calculated FE is −1.63 {−1.63} eV/Pt, 0.15 eV lower than the tabulated standard heat of formation of −1.48 eV/Pt.^{65,66} Wang et al. assigned an IR absorption peak at 840 cm^{−1} to PtO molecules trapped in a neon matrix,⁶⁷ in close agreement with our results. The most stable Pt₂O₂ isomer is obtained by joining two PtO's in a head-to-tail arrangement (Figure 3) and has an FE of −1.72 {−1.69} eV/Pt. The Pt–Pt distance is elongated by 0.23 Å relative to the Pt dimer (2.34 Å), and the Pt–O bonds are between 1.7 and 2.0 Å. In comparison, the calculated nearest Pt–Pt and Pt–O distances in bulk PtO are 3.14 and 2.08 Å, respectively, both of which are considerably longer than their counterparts in the PtO and Pt₂O₂ cluster.

TABLE 2: Net Spin and Bader Atomic Charges of Pt_xO_x Clusters

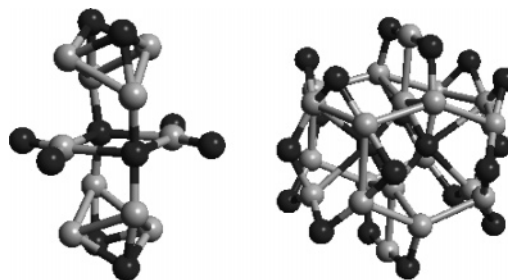
cluster	spin		charge (e) ^a
PtO	2	Pt	+0.48
		O	-0.48
Pt ₂ O ₂	0	Pt	+0.99 ± 0.36
		O	-0.70 - 0.65
Pt ₃ O ₃	2	Pt	+0.77 ± 0.01
		O	-0.77 ± 0.02
Pt ₄ O ₄	0	Pt	+0.77 ± 0.02
		O	-0.77 ± 0.01
Pt ₅ O ₅	2	Pt	+0.76 ± 0.02
		O	-0.76 ± 0.02
Pt ₁₀ O ₁₀	0	Pt	+0.76 ± 0.19
		O	-0.76 ± 0.05
bulk PtO	0	Pt	+0.96 ± 0.00
		O	-0.96 ± 0.00

^a For the sake of clarity, when there is more than one Pt or O atom in a cluster or unit cell (for bulk), the average charge is reported with the standard deviation except for asymmetric Pt₂O₂, for which the individual values are presented.

**Figure 3.** Relative stability of Pt_xO_x isomers ($x = 1-5$) and their stick-and-ball representations. Select bond lengths (in Å) and angles (in deg) of the most stable structure are as indicated.

Bader charge analysis reveals another difference between the molecular and bulk PtO (see Table 2): The extent of charge transfer from Pt to O in the PtO cluster is only about half of that in bulk PtO, indicating more covalent character in the former. Pt₂O₂ has an asymmetric structure, so its two Pt atoms are not equivalent. The middle Pt atom, because it is bonded to two O atoms, is more oxidized (+0.96) than the terminal Pt atom, bonded to only one O atom (+0.35). Isomers containing O₂ ligands are all considerably less stable than if the two O atoms are separate, indicating that the dissociation of O₂ is energetically favored on the Pt dimer.

The most stable Pt₃O₃, Pt₄O₄, and Pt₅O₅ clusters share a common characteristic: They can all be viewed as being formed

**Figure 4.** Pt₁₀O₁₀ cluster.**Figure 5.** Bulk fragments with Pt₁₀O₁₀ (left) and Pt₂₀O₂₀ (right) compositions.

by an increasing number of PtO units connected head-to-tail, in which single O atoms bridge elongated Pt-Pt bonds, creating rings that preserve Pt coordination to two O atoms. In contrast, Pt is 4-fold coordinated in PtO and β -PtO₂ bulk oxides. The most stable Pt₃O₃ cluster (Figure 3) is an equilateral triangle with an FE of -1.77 [-1.73] eV/Pt, at least 0.5 eV/cluster more stable than those in which some O atoms occupy terminal (O_{term}) or 3-fold positions and than those with open Pt backbones. The Pt-Pt distance is 2.63 Å, 0.13 Å longer than the edges of the Pt₃ cluster. The Pt atoms in the most stable Pt₄O₄ cluster (Figure 3) form a slightly twisted parallelogram. This cluster has an FE of -1.92 [-1.88] eV/Pt. Here, the Pt atoms abandon the tetrahedral configuration of the Pt₄ cluster and instead adopt a planar geometry. Although our calculations show that the tetrahedral Pt₄ is 0.28 eV more stable than planar Pt₄, Pt₄O₄ isomers in which the Pt atoms retain the tetrahedral arrangement are substantially less stable than the preferred ring structure (see isomers in Figure 3). For Pt₅O₅, the most stable structure is a bent pentagon with an FE of -1.88 [-1.84] eV/Pt. Like Pt₄O₄, the Pt atoms abandon the pyramidal configuration of the Pt₅ cluster. Apparently, significant stabilization is gained when the O atoms are fully coordinated and spatially separated and when no Pt atom binds more than two O atoms at once. The extent of electron transfer from Pt to O (Table 2) suggests that the Pt-O bonds in the Pt₃O₃-Pt₅O₅ clusters remain less ionic than bulk PtO, although the level of ionicity is approaching the bulk as the cluster becomes larger.

To search for the minimum-energy Pt₁₀O₁₀ cluster, we followed the small cluster trend and optimized several large loop structures, the most stable of which looks like a hexagonal Pt₇ patch fused with a Pt₄ ring (Figure 4). The FE of this structure is -1.26 [-1.22] eV/Pt, which sets an upper limit for the global minimum on the Pt₁₀O₁₀ PES. The Pt-Pt bond lengths range from 2.6 to 3.0 Å, and the Pt-O bonds are between 1.8 and 2.0 Å long.

The stability of this series of loop structures is initially surprising, as one might expect the clusters to tend toward the compact structure and higher Pt coordination of the bulk oxide as they grew in size. As a test, we calculated a Pt₁₀O₁₀ and a Pt₂₀O₂₀ fragment extracted from bulk PtO (Figure 5). After relaxation, the two fragments have FE's of -0.08 and -0.33

TABLE 3: Net Spin and Bader Atomic Charges of Pt_xO_{2x} Clusters

cluster	spin		charge (e) ^a
PtO_2	0	Pt	+1.27
		O	-0.63 ± 0.00
Pt_2O_4	0	Pt	+1.30 \pm 0.02
		O	-0.65 ± 0.03
Pt_3O_6	0	Pt	+1.29 \pm 0.02
		O	-0.65 ± 0.05
Pt_4O_8	2	Pt	+1.36 \pm 0.02
		O	-0.68 ± 0.05
Pt_5O_{10}	0	Pt	+1.39 \pm 0.08
		O	-0.69 ± 0.06
$\text{Pt}_{10}\text{O}_{20}$	0	Pt	+1.41 \pm 0.04
		O	-0.71 ± 0.02
bulk PtO_2	0	Pt	+1.70 \pm 0.00
		O	-0.85 ± 0.00

^a For the sake of clarity, when there is more than one Pt or O atom in the cluster or unit cell (for bulk), the average charge is reported with the standard deviation.

eV/Pt, respectively, higher even than the heat of formation of bulk PtO (-0.54 eV/Pt). (Pt_{20} energy is estimated using the fitted function mentioned before.) Therefore, we conclude that Pt_xO_x clusters with bulklike structures are favorable only at sizes much larger than those considered here.

Pt_xO_{2x} Clusters. We now turn our attention to the Pt_xO_{2x} clusters. The smallest of these, PtO_2 , prefers a linear O–Pt–O configuration and has a Pt–O bond length of 1.72 Å. The FE of PtO_2 is calculated to be -4.02 { -3.98 } eV/Pt (Table 3), in close agreement with the tabulated value of -4.12 eV.⁴⁹ Wang et al. assigned an IR absorption peak at 959 cm^{-1} ⁶⁷ to the anti-symmetric OPtO stretching mode, in close agreement with our calculated frequency of 980 cm^{-1} for this mode.

The preference for bridging O (O_{br}) atoms in Pt_2O_2 persists in Pt_2O_4 : The most favorable configuration for Pt_2O_4 has two of each (Figure 6). This somewhat puckered cluster has an FE of -2.68 { -2.61 } eV/Pt and is 0.2 eV/cluster more stable than the flat conformer (the one next to the puckered cluster in Figure 6). The Pt–Pt bond is 0.43 Å longer than in Pt_2 and 0.20 Å longer than in Pt_2O_2 but shorter than the Pt–Pt distance in bulk Pt_2O (3.62 Å). The Pt–O bonds (1.94 Å for Pt– O_{br} and 1.74 Å for Pt– O_{term}) are shorter than those in the bulk as well (2.04 Å).

By attaching more PtO_2 units to it the Pt_2O_4 cluster grows into the preferred, chainlike Pt_3O_6 , Pt_4O_8 , and Pt_5O_{10} clusters. The most stable Pt_3O_6 (Figure 6) cluster has an arched appearance and an FE of -2.38 { -2.29 } eV/Pt, whereas the straight conformer is ~ 0.3 eV/cluster less stable. Several bent Pt_4O_8 chains all lie within ~ 0.4 eV/cluster of one another. In particular, the curved (the rightmost one in the Pt_4O_8 panel, Figure 6) and the arched (third from the left) chains are nearly isoenergetic at -2.33 { -2.25 } eV/Pt. In the curved chain, the distance between the two middle Pt atoms has increased from 2.75 Å in Pt_3O_6 to 3.01 Å. The arched Pt_5O_{10} chain is the lowest in energy among various isomers with an FE of -2.23 { -2.15 } eV/Pt. It is more stable than the curved (third from the left) and the straight (second from the left) chains by up to 0.2 eV/cluster.

As expected, Bader analysis shows that the amount of positive charge on each Pt atom is twice the amount of negative charge on each O atom in the Pt_xO_{2x} clusters (see Table 3). As in the Pt_xO_x clusters, the Pt–O bonds in these small Pt_xO_{2x} clusters appear to be more covalent than those in bulk β - PtO_2 , and the level of ionicity similarly approaches the bulk level as the size of the cluster increases.

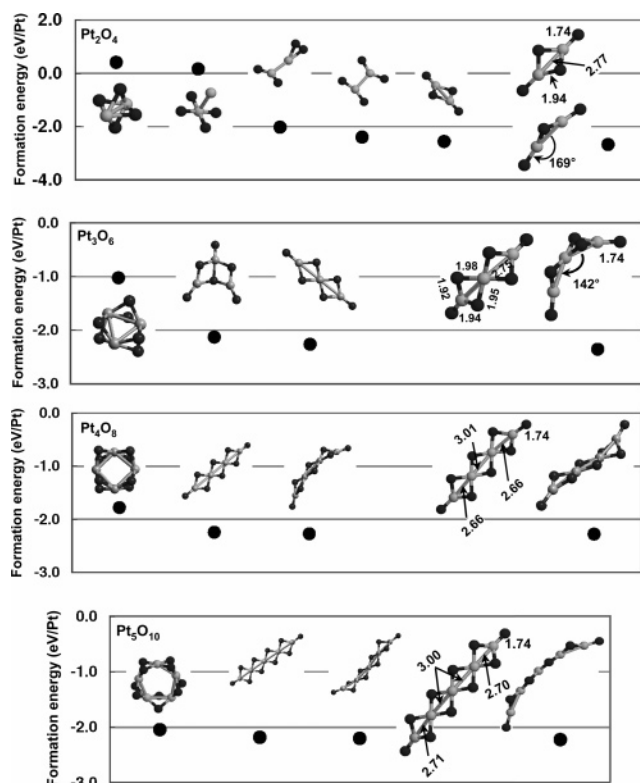


Figure 6. Relative stability of the Pt_xO_{2x} isomers, with the minimum-energy structures shown on the right. Select bond lengths (in Å) and angles (in deg) are as indicated.

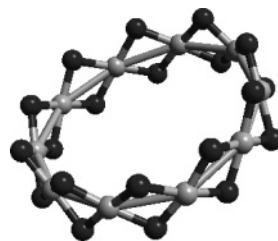


Figure 7. $\text{Pt}_{10}\text{O}_{20}$ ring.

As shown in Figure 6, a different series of Pt_xO_{2x} clusters can be formed by adding more O atoms to the bridge positions of the most stable Pt_xO_x clusters, creating closed loops instead of linear chains. If three additional O atoms are thus added to the most stable Pt_3O_3 cluster (Figure 3), the resultant triangular structure would be less stable than the Pt_3O_6 chain by ~ 4 eV/cluster. As the length of the Pt backbone increases, the energetic difference between the closed loops and their linear counterparts narrows. Adding four more O atoms to the bridge positions of the Pt_4O_4 cluster (Figure 3) creates an isomer that is ~ 2 eV/cluster less stable than the Pt_4O_8 chain, and a similarly formed Pt_5O_{10} ring is 0.9 eV/cluster less stable than the Pt_5O_{10} chain. Somewhere between Pt_5O_{10} and $\text{Pt}_{10}\text{O}_{20}$, the chain structure becomes long and flexible enough so that closed loops can form to allow the terminal Pt atoms to be fully coordinated, which is energetically favorable and now outweighs the penalty associated with constraining the Pt backbone. The large ring shown in Figure 7 is lower in energy than the most stable chain that we can find for $\text{Pt}_{10}\text{O}_{20}$, but only by less than 1 eV/cluster. The FE of this $\text{Pt}_{10}\text{O}_{20}$ ring is -1.80 { -1.72 } eV/Pt.

Again, to contrast the chains and loops described above with more compact clusters, we consider two fragments extracted from bulk β - PtO_2 : one with Pt_7O_{14} and the other with $\text{Pt}_{11}\text{O}_{22}$ composition (Figure 8). Their FE is -0.53 and -0.68 eV/Pt,

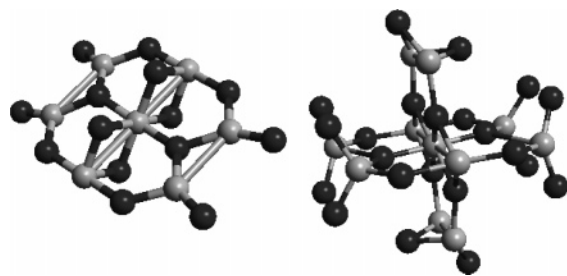


Figure 8. Bulk fragments with Pt_7O_{14} (left) and $\text{Pt}_{11}\text{O}_{22}$ (right) compositions.

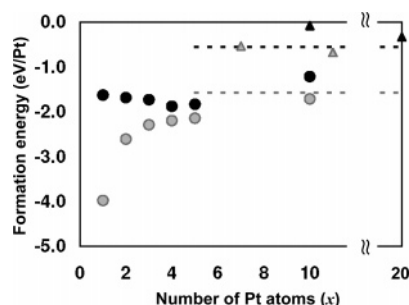


Figure 9. Formation energies (ZPE-corrected) of the most stable Pt_xO_x (●) and Pt_xO_{2x} (○) clusters. The formation energies of the bulk-like PtO fragments (▲) and PtO_2 fragments (△) and of bulk PtO (−0.55 eV) and $\beta\text{-PtO}_2$ (−1.57 eV) (black and gray dashed lines, respectively) are also included for comparison.

respectively, on the basis of estimated total energies for Pt_7 and Pt_{11} . Thus, similar to the Pt_xO_x bulk fragments, these clusters are less stable than bulk $\beta\text{-PtO}_2$, the FE of which is −1.57 eV/Pt, and are, therefore, still less stable than the loop or chain isomers of the same compositions.

Discussion

As shown in Figure 9, the calculated Pt_xO_x and Pt_xO_{2x} formation energies reveal several important characteristics: The small clusters have much lower FE's than the heats of formation of respective bulk PtO or PtO_2 . In fact, the oxidation of a Pt atom or Pt dimer is over 1 eV/Pt more exothermic than the formation of the bulk oxides. As the size of the cluster increases, the FE approaches the respective bulk levels (oxidation becoming less exothermic). Thus, the smaller the Pt cluster, the greater its affinity for oxygen. This suggests that the traditional approach of correlating the catalytic activity of metal oxides with bulk heats of formation⁶⁸ would be inappropriate for small metal oxide clusters.

There are also some important differences between the two series of Pt–oxide clusters. The FE's of the Pt_xO_{2x} clusters always lie beneath those of the Pt_xO_x clusters, so on the basis of electronic energy alone (although not necessarily thermodynamically), Pt clusters prefer to be completely, rather than partially, oxidized. Whereas the FE's of the Pt_xO_{2x} clusters rise quickly and asymptotically toward the bulk PtO_2 level, the FE's of the Pt_xO_x clusters appear to form a minimum at Pt_4 before rising, more gradually, toward the bulk PtO level. The partial oxidation of Pt_x clusters in the vicinity of $x = 4$ is, therefore, easier than the formation of smaller or larger Pt_xO_x clusters. The difference in FE between the two oxidation states, which corresponds to the reaction energy for $\text{Pt}_x\text{O}_x + (x/2)\text{O}_2 \rightarrow \text{Pt}_x\text{O}_{2x}$, also varies over a wide range, from approximately 2 eV/Pt for a single Pt to less than 0.4 eV at Pt_4 , ultimately widening to the 1 eV/Pt characteristic of the bulks. Because the energetic advantage of complete oxidation over partial oxidation is quite

small in this size range, these partially oxidized clusters (Pt_4O_4 , Pt_5O_5 , and perhaps Pt_6O_6) may persist over a wider range of conditions than smaller or larger Pt_xO_x clusters. This is a clear demonstration of a nanoscale effect, one that has implications for the stability and reactivity of clusters as functions of size. Similar effects may well exist for other metals and may contribute, for instance, to the dramatic size effects observed in Au nanoclusters.

It is evident from the preceding figures that structurally these Pt–oxide nanoclusters also differ substantially from the corresponding bulk Pt–oxides. Whether open or looped, structures much more extensive in one dimension than the others are preferred. It remains to be seen whether these unique structures can be detected experimentally. The small bulk fragments mentioned before ($\text{Pt}_{10}\text{O}_{10}$, $\text{Pt}_{20}\text{O}_{20}$, Pt_7O_{14} , and $\text{Pt}_{11}\text{O}_{22}$) are all less stable than even the bulk oxides, and their FE's approach the bulk oxide levels from the opposite side (Figure 9). The reason may be the excess surface energy of a fragment compared to the bulk. One may infer from the figure that the three-dimensional structures of the bulk oxides will not begin to prevail until probably $x \geq 20$.

It is worth noting that, unlike oxide clusters of oxophilic early transition metals such as vanadium (V), the Pt–Pt bonds in the smaller Pt–oxide clusters are not broken by oxidation. Their length is usually smaller than or comparable to the Pt–Pt distance in the bulk metal phase, 2.83 Å (the experimental value is 2.77 Å). Whereas gas-phase V oxide clusters are thought to possess no direct V–V linkage,^{69,70} we find no energetic advantage for O insertion into Pt–Pt bonds (cf. Figure 3). The reason may be that the V–O bond is about 3 eV stronger than the V–V bond, whereas the Pt–O and Pt–Pt bonds are of comparable strength as evidenced by the AE of the PtO and Pt_2 molecules (3.82⁴⁹ and 3.14 eV,⁶³ respectively). The large differential in metal–metal and metal–oxygen bonds may also account for the loss of metal bonds in the smallest aluminum oxide⁷¹ and titanium oxide⁷² clusters. As the Pt atoms become more oxidized in the larger clusters (e.g., see $\text{Pt}_{10}\text{O}_{10}$ and $\text{Pt}_4\text{O}_8\text{--Pt}_{10}\text{O}_{20}$), Pt–Pt bonds are gradually lost. The bulk oxides possess no direct Pt–Pt bonds as the Pt–Pt distance is well over 3 Å.

Conclusions

Self-consistent periodic DFT calculations (GGA-PW91) have been performed to study a series of free Pt_x , Pt_xO_x , and Pt_xO_{2x} nanoclusters ($x = 1, 2, 3, 4, 5$, and 10). The calculated geometry and atomization energies of the Pt_x clusters are in good agreement with previous theoretical findings and available experimental data. In particular, the atomization energy per Pt atom is found to increase with increasing cluster size.

The Pt_xO_x clusters ($x > 2$) prefer to form closed loops, in which the Pt atoms comprise the backbones in the shape of triangle, quadrangle, pentagon, etc. with each O atom occupying a Pt–Pt bridge position and each Pt atom coordinated to two O atoms. The Pt_xO_{2x} series, on the other hand, form various curved linear chain structures, in which each middle Pt atom is coordinated to four O atoms and each terminal Pt atom coordinated to three. At a certain length, the chain structure becomes flexible enough to form a closed loop so that all the Pt atoms are fully coordinated. Therefore, both the Pt_xO_x and Pt_xO_{2x} clusters prefer what may be loosely described as one- or two-dimensional structures, as opposed to the three-dimensional matrices of the bulk oxides or the Pt metal.

Our results show that discrete Pt clusters are more readily oxidized than bulk Pt and that the smaller the Pt cluster, the

more readily it is oxidized. The FE's of the Pt_xO_{2x} clusters rise monotonically and approach the bulk PtO_2 level asymptotically, whereas the FE's of the Pt_xO_x clusters pass through a minimum around $x = 4$ before rising, more gradually, toward the bulk PtO energy. Complete oxidation of Pt_x (to Pt_xO_{2x}) is always favored energetically over partial oxidation (to Pt_xO_x) regardless of the cluster size. Bader analysis reveals that the Pt—O bonds in the Pt_xO_x and Pt_xO_{2x} clusters have considerable covalent character compared to the bulk oxides. Therefore, structurally, energetically, and chemically, the Pt—oxide nanoclusters are distinctly different states from the bulk Pt—oxides.

The implications of these findings for heterogeneous catalysis are worth considering. First, it is clear that Pt oxidation will be more important in few-atom clusters than in larger, bulklike particles and extended surfaces. This oxidation could be relevant not only to the particle composition but also to its interactions with supports. Second, because the energetics of the $\text{Pt}_x \rightarrow \text{Pt}_x\text{O}_x$ and $\text{Pt}_x\text{O}_x \rightarrow \text{Pt}_x\text{O}_{2x}$ transformations depend strongly on and vary nonlinearly with x , the few-atom clusters are anticipated to exhibit disparate activities for catalytic oxidation compared to bulk Pt. Exploration of these structural and catalytic effects is the topic of ongoing computational and experimental efforts.

Acknowledgment. This research is sponsored by the Office of Energy Efficiency and Renewable Energy of the U.S. Department of Energy (DOE). The work has been performed at Oak Ridge National Laboratory (ORNL), which is managed by UT-Battelle, LLC under DOE Contract No. DE-AC05-00OR22725, and used resources of the Center for Computational Sciences at ORNL. We thank Rachel Getman for her valuable help.

References and Notes

- (1) Vielstich, W.; Lamm, A.; Gasteiger, H. A. *Handbook of Fuel Cells: Fundamentals, Technology, Applications*; Wiley: West Sussex, 2003.
- (2) Gandhi, H. S.; Graham, G. W.; McCabe, R. W. *J. Catal.* **2003**, *216*, 433.
- (3) Bagot, P. A. *J. Mater. Sci. Technol.* **2004**, *20*, 679.
- (4) Satterfield, C. *Heterogeneous catalysis in industrial practice*, 2nd ed.; McGraw-Hill: New York, 1991.
- (5) Haruta, M.; Date, M. *Appl. Catal., A* **2001**, *222*, 427.
- (6) Lopez, N.; Janssens, T. V. W.; Clausen, B. S.; Xu, Y.; Mavrikakis, M.; Bligaard, T.; Nørskov, J. K. *J. Catal.* **2004**, *223*, 232.
- (7) Molina, L. M.; Hammer, B. *Phys. Rev. Lett.* **2003**, *90*, 206102.
- (8) Liu, Z. P.; Jenkins, S. J.; King, D. A. *Phys. Rev. Lett.* **2005**, *94*, 196102.
- (9) Boyen, H. G.; Kastle, G.; Weigl, F.; Koslowski, B.; Dietrich, C.; Ziemann, P.; Spatz, J. P.; Riethmüller, S.; Hartmann, C.; Möller, M.; Schmid, G.; Garnier, M. G.; Oelhafen, P. *Science* **2002**, *297*, 1533.
- (10) Lauritsen, J. V.; Bollinger, M. V.; Lægsgaard, E.; Jacobsen, K. W.; Nørskov, J. K.; Clausen, B. S.; Topsøe, H.; Besenbacher, F. *J. Catal.* **2004**, *221*, 510.
- (11) Ovesson, S.; Lundqvist, B. I.; Schneider, W. F.; Bogicevic, A. *Phys. Rev. B: Condens. Matter Mater. Phys.* **2005**, *71*, 115406.
- (12) Parks, E. K.; Weiller, B. H.; Bechthold, P. S.; Hoffman, W. F.; Nieman, G. C.; Pobo, L. G.; Riley, S. J. *J. Chem. Phys.* **1987**, *88*, 1622.
- (13) Xu, Z. T.; Rheingold, A. L.; Gates, B. C. *J. Phys. Chem.* **1993**, *97*, 9465.
- (14) Gates, B. C. *Chem. Rev.* **1995**, *95*, 511.
- (15) Enderle, B.; Gates, B. C. *J. Mol. Catal. A: Chem.* **2003**, *204*, 473.
- (16) Lamb, H. H.; Wolfer, M.; Gates, B. C. *J. Chem. Soc., Chem. Commun.* **1990**, *19*, 1296.
- (17) Bhirud, V.; Goellner, J. F.; Argo, A. M.; Gates, B. C. *J. Phys. Chem. B* **2004**, *108*, 9752.
- (18) Argo, A. M.; Gates, B. C. *J. Phys. Chem. B* **2003**, *107*, 5519.
- (19) Argo, A. M.; Odzak, J. F.; Gates, B. C. *J. Am. Chem. Soc.* **2003**, *125*, 7107.
- (20) Larsen, G.; Haller, G. L. *Catal. Lett.* **1989**, *3*, 103.
- (21) Chang, J. R.; Koningsberger, D. C.; Gates, B. C. *J. Am. Chem. Soc.* **1992**, *114*, 6460.
- (22) Davis, R. J. *Heterog. Chem. Rev.* **1994**, *1*, 41.
- (23) Fierro-Gonzalez, J. C.; Gates, B. C. *J. Phys. Chem. B* **2004**, *108*, 16999.
- (24) Lee, S.; Fan, C.; Wu, T.; Anderson, S. L. *J. Am. Chem. Soc.* **2004**, *126*, 5682.
- (25) Reuter, K.; Stampfl, C.; Ganduglia-Pirovano, M. V.; Scheffler, M. *Chem. Phys. Lett.* **2002**, *352*, 311.
- (26) Reuter, K.; Frenkel, D.; Scheffler, M. *Phys. Rev. Lett.* **2004**, *93*, 116105.
- (27) Li, W.-X.; Stampfl, C.; Scheffler, M. *Phys. Rev. Lett.* **2003**, *90*, 256102.
- (28) Bocquet, M.-L.; Michaelides, A.; Loffreda, D.; Sautet, P.; Alavi, A.; King, D. A. *J. Am. Chem. Soc.* **2003**, *125*, 5620.
- (29) Bocquet, M.-L.; Sautet, P.; Cerda, J.; Carlisle, C. I.; Webb, M. J.; King, D. A. *J. Am. Chem. Soc.* **2003**, *125*, 3119.
- (30) McBride, J. R.; Graham, G. W.; Peters, C. R.; Weber, W. H. *J. Appl. Phys.* **1991**, *69*, 1596.
- (31) Deutsch, S. E.; Miller, J. T.; Tomishige, K.; Iwasawa, Y.; Weber, W. A.; Gates, B. C. *J. Phys. Chem.* **1996**, *100*, 13408.
- (32) Held, G.; Jones, L. B.; Seddon, E. A.; King, D. A. *J. Phys. Chem. B* **2005**, *109*, 6159.
- (33) Alexeev, O. S.; Li, F.; Amiridis, M. D.; Gates, B. C. *J. Phys. Chem. B* **2005**, *109*, 2338.
- (34) Hendriksen, B. L. M.; Frenken, J. W. M. *Phys. Rev. Lett.* **2002**, *89*, 046101.
- (35) Li, W. X.; Osterlund, L.; Vestergaard, E. K.; Vang, R. T.; Matthiesen, J.; Pedersen, T. M.; Laegsgaard, E.; Hammer, B.; Besenbacher, F. *Phys. Rev. Lett.* **2004**, *93*.
- (36) Ackermann, M. D.; Pedersen, T. M.; Hendriksen, B. L. M.; Robach, O.; Bobaru, S. C.; Popa, I.; Quiros, C.; Kim, H.; Hammer, B.; Ferrer, S.; Frenken, J. W. M. *Phys. Rev. Lett.* **2005**, *95*.
- (37) Wang, J. G.; Li, W. X.; Borg, M.; Gustafson, J.; Mikkelsen, A.; Pedersen, T. M.; Lundgren, E.; Weissenrieder, J.; Kiklovits, J.; Schmid, M.; Hammer, B.; Andersen, J. N. *Phys. Rev. Lett.* **2005**, *95*.
- (38) Campbell, C. T.; Parker, S. C.; Starr, D. E. *Science* **2002**, *298*, 811.
- (39) Zemski, K. A.; Justes, D. R.; Castleman, A. W. *J. Phys. Chem. B* **2002**, *106*, 6136.
- (40) Kresse, G.; Furthmüller, J. *Comput. Mater. Sci.* **1996**, *6*, 15.
- (41) Kresse, G.; Furthmüller, J. *Phys. Rev. B: Condens. Matter Mater. Phys.* **1996**, *54*, 11169.
- (42) Kresse, G.; Hafner, J. *Phys. Rev. B: Condens. Matter Mater. Phys.* **1994**, *49*, 14251.
- (43) Kresse, G.; Hafner, J. *Phys. Rev. B: Condens. Matter Mater. Phys.* **1993**, *47*, 558.
- (44) Perdew, J. P.; Chevary, J. A.; Vosko, S. H.; Jackson, K. A.; Pederson, M. R.; Singh, D. J.; Fiolhais, C. *Phys. Rev. B: Condens. Matter Mater. Phys.* **1992**, *46*, 6671.
- (45) Vanderbilt, D. *Phys. Rev. B: Condens. Matter Mater. Phys.* **1990**, *41*, 7892.
- (46) Blöchl, P. E.; Jepsen, O.; Andersen, O. K. *Phys. Rev. B: Condens. Matter Mater. Phys.* **1994**, *49*, 16223.
- (47) Kittel, C. *Introduction to Solid State Physics*, 7th ed.; Wiley: New York, 1996.
- (48) Kaye, G. W. C.; Laby, T. H. *Tables of physical and chemical constants*, 16th ed.; Longman: Essex, England, 1995.
- (49) *The Oxide Handbook*; IFI/Plenum: New York, 1973.
- (50) Ashcroft, N. W.; Mermin, N. D. *Solid State Physics*; Saunders College: Orlando, FL, 1976.
- (51) Range, K.-J.; Rau, F.; Klement, U.; Heyns, A. M. *Mater. Res. Bull.* **1987**, *22*, 1541.
- (52) Nosé, S. *J. Chem. Phys.* **1984**, *81*, 511.
- (53) Bader, R. F. W. *Atoms in Molecules—A Quantum Theory*; Oxford University Press: Oxford, 1990.
- (54) Henkelman, G.; Arnaldsson, A.; Jónsson, H. *Comput. Mater. Sci.* In press.
- (55) Majumdar, D.; Dai, D.; Balasubramanian, K. *J. Chem. Phys.* **2000**, *113*, 7928.
- (56) Majumdar, D.; Dai, D.; Balasubramanian, K. *J. Chem. Phys.* **2000**, *113*, 7919.
- (57) Lin, X.; Ramer, N. J.; Rappe, A. M.; Hass, K. C.; Schneider, W. F.; Trout, B. L. *J. Phys. Chem. B* **2001**, *105*, 7739.
- (58) Anton, J.; Jacob, T.; Fricke, B. *Phys. Rev. Lett.* **2002**, *89*, 213001.
- (59) Sebetci, A.; Güvenç, Z. B. *Surf. Sci.* **2002**, *525*, 66.
- (60) Xiao, L.; Wang, L. C. *J. Phys. Chem. A* **2004**, *108*, 8605.
- (61) Airola, M. B.; Morse, M. D. *J. Chem. Phys.* **2002**, *116*, 1313.
- (62) Ho, J.; Polak, M. L.; Ervin, K. M.; Lineberger, W. C. *J. Chem. Phys.* **1993**, *99*, 8542.
- (63) Tayler, S.; Lemire, G. W.; Hamrick, Y. M.; Fu, Z.; Morse, M. D. *J. Chem. Phys.* **1988**, *89*, 5517.
- (64) de Silva, A. P.; Gunaratne, H. Q. N.; Gunnlaugsson, T.; Huxley, A. J. M.; McCoy, C. P.; Rademacher, J. T.; Rice, T. E. *Chem. Rev.* **1997**, *97*, 1515.

- (65) Pankratz, L. B. *Thermodynamic properties of carbides, nitrides, and other selected substances*; U. S. Department of the Interior, U. S. Bureau of Mines, 1995.
- (66) *CRC Handbook of Chemistry and Physics*, 83rd ed.; CRC Press: Boca Raton, FL, 2002.
- (67) Wang, X. F.; Andrews, L. *J. Phys. Chem. A* **2001**, *105*, 5812.
- (68) Klier, K. *J. Catal.* **1967**, *8*, 14.
- (69) Bell, R. C.; Zemski, K. A.; Justes, D. R.; Castleman, A. W. *J. Chem. Phys.* **2001**, *114*, 798.
- (70) Matsuda, Y.; Bernstein, E. R. *J. Phys. Chem. A* **2005**, *109*, 3803.
- (71) Ghanty, T. K.; Davidson, E. R. *J. Phys. Chem. A* **1999**, *103*, 8985.
- (72) Hamad, S.; Catlow, C. R. A.; Woodley, S. M.; Lago, S.; Mejías, J. A. *J. Phys. Chem. B* **2005**, *109*, 15741.